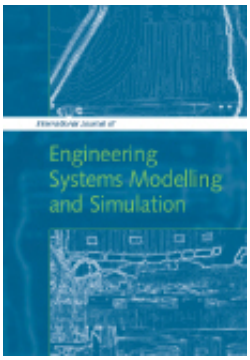

International Journal of Engineering Systems Modelling and Simulation

ISSN online: 1755-9766 - ISSN print: 1755-9758
https://www.inderscience.com/ijesms

Research on numerical simulation of wind load on high-rise buildings along the street based on BIM model

Lianguang Mo, Wenying Lu

DOI: 10.1504/IJESMS.2025.10067651

Article History:

Received:	24 December 2020
Last revised:	24 December 2020
Accepted:	01 October 2023
Published online:	02 December 2024

Research on numerical simulation of wind load on high-rise buildings along the street based on BIM model

Lianguang Mo

College of Management,
Hunan City University,
Yiyang, 413000, China
Email: molianguang12@sina.com

Wenying Lu*

School of Architectural Decoration,
Jiangsu Vocational Institute of Architectural Technology,
Xuzhou, 221116, China
Email: wenying@mls.sinanet.com
*Corresponding author

Abstract: In order to overcome the problems of poor accuracy and low efficiency in the existing numerical simulation methods of building surface wind load, a new numerical simulation method of high-rise street building surface wind load based on BIM model is proposed. This method obtains the data of high-rise buildings along the street based on BIM model, and selects Realisable k-ε model as the turbulence model. The non-equilibrium wall function method is used to deal with the turbulence state on the building surface, the boundary conditions are set, and the turbulence model is calculated and solved by a separate solver to realise the numerical simulation of the surface wind load of high-rise street buildings. The experimental results show that the average error of the wind pressure coefficient of the proposed numerical simulation method is less than 0.4, which fully shows that the proposed numerical simulation method has good performance.

Keywords: BIM model; high-rise buildings along the street; building surface; wind load; numerical simulation.

Reference to this paper should be made as follows: Mo, L. and Lu, W. (2025) 'Research on numerical simulation of wind load on high-rise buildings along the street based on BIM model', *Int. J. Engineering Systems Modelling and Simulation*, Vol. 16, No. 1, pp.52–62.

Biographical notes: Lianguang Mo has a PhD in Applied Economics. He graduated from School of Finance and Taxation, Zhongnan University of Economics and Law. He is an Associate Professor of Department of City Management, Hunan Urban University. His research interests are intelligent control and project management.

Wenying Lu received her degree of Master of Arts from Soochow University in 2007. Currently, she is an Associate Professor in the School of Architectural Decoration of Jiangsu Vocational Institute of Architectural Technology. Her research interests include decorative arts of the Han Dynasty, exhibition design.

1 Introduction

Wind is a common natural phenomenon, mainly by the horizontal pressure gradient force, resulting in air flow, thus forming wind. Under normal circumstances, the breeze will bring people a comfortable feeling. But if the wind intensity is too high, it will form a wind disaster, causing the loss of human life and property (Li et al., 2018a). According to the statistical yearbook data, in natural disasters, the economic loss caused by wind disaster and its proportion occupy the first place. When the wind meets the structural obstacles, it will produce a certain pressure, which will cause the structure to vibrate and deform under the pressure. If the vibration and deformation of the structure exceeds its own bearing capacity, the structure will be damaged locally or completely and can not work normally. Through statistical research, it is found that the wind disaster mainly occurs in the destruction or collapse of engineering structures (Mansur et al., 2018). In recent years, China's high-rise buildings have sprung up like bamboo shoots after a spring rain, and the resulting wind disaster events are also increasing. For high-rise buildings, wind load is a very

critical load, which is an indispensable factor in the process of structural design of high-rise buildings. With the emergence of a large number of high-rise and super high-rise buildings, wind load also plays a more and more important role and becomes the control load of high-rise building structure design. In particular, the surface of high-rise buildings along the street is subject to greater wind force, with higher risk. Therefore, how to determine the wind pressure on the surface of high-rise buildings along the street is very important to further study the effect of wind on building structure (Wang et al., 2018).

Lv and Liu (2019) puts forward the numerical simulation method of wind load on the surface of high-rise Street buildings based on the separated vortex method. In this method, the separated vortex model is constructed for large eddy simulation, and the turbulent boundary conditions of wind field of high-rise Street buildings are simulated by turbulent pulsating flow. The wind pressure distribution characteristics around high-rise Street buildings are calculated respectively, and the simulation results of wind load on the building surface are obtained. However, this method can not build the grid model of elevation building, resulting in low simulation accuracy. Chen et al. (2019) proposes a numerical simulation method of wind load on the surface of high-rise Street buildings based on three-dimensional digital photogrammetry technology. In this method, double cameras are used to measure the actual wind load image of high-rise Street buildings, and three-dimensional digital photogrammetry deformation measurement technology is used to obtain the strain and deflection of buildings under different wind loads, complete the numerical simulation of wind load of high-rise Street buildings. However, due to the unreasonable boundary conditions of the turbulence model, the accuracy of the simulation results is insufficient. Zheng et al. (2018) proposes a numerical simulation method of wind load on the surface of high-rise Street buildings based on ANSYS finite element analysis method. This method first collects the variable of wind load parameters of high-rise Street buildings, and uses the finite element model for numerical simulation research according to this variable, but the simulation accuracy of this method still needs to be further improved.

In order to solve the problems of the above methods, a numerical simulation method for wind load on the surface of high-rise buildings along the street based on BIM model is proposed. The overall scheme of this method is as follows:

1 BIM model is used to accurately collect the data of windows and walls of high-rise buildings along the street, and the model of high-rise buildings along the street is constructed according to the data.

2 Based on the above model, the realisable model is selected as the turbulence model, and the non-equilibrium wall function method is used to obtain the turbulent state of the building surface.

3 The flow around the building is divided into unstructured grids, boundary conditions are set, and the turbulence model is solved to realise the numerical simulation of wind load on the surface of high-rise buildings along the street.

Through the above scheme, the accurate and rapid simulation of wind load on the surface of high-rise buildings along the street is realised.

2 Numerical simulation of wind load on the surface of high-rise buildings along the street

2.1 Data acquisition of high-rise buildings along the street based on BIM model

In order to improve the accuracy of numerical simulation of wind load on the surface of high-rise buildings along the street, the data of high-rise buildings along the street are extracted from BIM model to provide accurate data support for the establishment of the following high-rise buildings along the street.

Building information modelling takes the relevant information data of construction projects as the basis of the model, establishes the building model, and simulates the real information of the building through digital information simulation. It has eight characteristics: information completeness, information relevance, information consistency, visualisation, coordination, simulation, optimisation and plotting.

There are many types of data in BIM model, and there are many applications in BIM model, including the data of doors, windows, railings and other high-rise building components. Under normal circumstances, the BIM model data volume of a high-rise building component can reach about 200M. If the data of internal water supply and drainage, HVAC and other components are added, the BIM model will be more huge. BIM model data is integrated according to the properties of components, which greatly facilitates the extraction of high-rise buildings along the street.

The research object of this paper is the surface of high-rise buildings along the street, which mainly includes windows and walls. Revit software is one of BIM model software, which can generate the list of different types of components, eliminating the process of data pre-processing, greatly improving the speed of high-rise building data extraction (Shu et al., 2019). The surface data of high-rise buildings along the street extracted by the Revit software are shown in Table 1.

Through the above process, the surface data of high-rise buildings along the street are extracted, which mainly includes the detailed data of windows and walls of high-rise buildings, which is prepared for the establishment of the following high-rise buildings along the street.

Table 1 Surface data of high-rise buildings along the street

(1) Window schedule				
Window name or number	*Size*			*Total*
	Height (cm)	*Width (cm)*	*The measure of area (m2)*	
Single layer window with three columns	1,550	2,100	3	1
Single layer window with three columns	1,550	2,400	4	2
Casement window c0512	1,200	500	1	145
Casement window c0612	1,200	600	1	116
Casement window single layer	1,400	1,000	1	1
Casement window single layer	2,900	2,400	7	2
LC0918	1,800	900	2	1
LC0920	2,000	900	2	1
LC1120	2,000	1,100	2	1
LC1518	1,800	1,500	3	1
LC1520	2,000	1,500	3	1
LC1818	1,800	1,800	3	1
LC1820	2,000	1,800	4	4
LC2318	1,800	2,300	4	1
LC2320	2,000	2,300	5	2
LC2324	2,400	2,300	6	1
LC2524	2,400	2,500	6	1
TC0912	1,200	1,060	1	116
TC1119A	1,900	1,210	2	58
TC1519	1,900	1,660	3	116
TC1619	1,900	1,760	3	116
TC2019	1,900	2,160	4	58
TC2319	1,900	2,460	5	116
(2) Wall schedule				
Wall material details				
Material name	*Model*		*Material volume (m^3)*	
Plasterboard	-		88.04	
Concrete block	-		23.78	
Concrete pouring	C30		850.70	
Concrete pouring	C40		389.10	
Concrete pouring	C45		387.73	
Concrete pouring	C50		388.03	
Concrete pouring	C55		385.15	
Concrete pouring	C60		693.73	
Brick	Shale porous brick		2,431.44	
Brick	Fired shale hollow brick		160.86	
Brick	Thick wall shale hollow brick	3,935.00		

2.2 Building model of high-rise buildings along the street

In order to facilitate the research, according to the above extracted high-rise building surface data along the street, the model of high-rise building along the street is established. The specific model building process is as follows.

The full size of the high-rise building along the street is set to be 100 ft 150 ft 600 ft. In appearance, it is a simple rectangular building. The surface of the building is very flat, without any appendages, and there is no disturbance around the building (Mohammadi-Aragh et al., 2018). 20 pressure measuring points are arranged on the two-thirds height horizontal plane of the high-rise building model along the

street. The specific model and the arrangement of pressure measuring points are shown in Figure 1.

Figure 1 Model of high-rise buildings along the street and layout of pressure measuring points

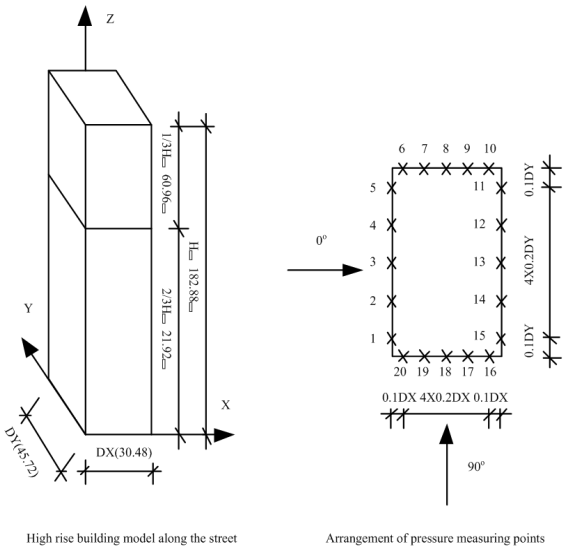

The above process completes the building model of high-rise buildings along the street, and arranges the pressure test points. During the research process, it is considered that the whole atmospheric environment is simulated in this area.

2.3 Turbulence model selection

At present, the turbulence models used in numerical simulation include Reynolds stress model, k–ε model, Realisable k–ε model and large eddy simulation model (Caroline and Muller, 2018). Through comparative study, it is found that realisable k–ε model is an improvement of k–ε model, which is mainly reflected in the value of isotropic turbulence viscosity assumption (i.e., C_μ parameter) and dissipation rate control equation. The C_μ parameter of realisable k–ε model is no longer simply a constant, but combined with the average velocity gradient, it can reflect the anisotropy of turbulence more comprehensively. The realisable k–ε model has higher accuracy in the simulation of flow around bluff body. Therefore, this model is selected as the turbulence model. The turbulent energy consumption parameter is assumed to be A_0 = 4.0. The dispersion parameter is

$$A_s = \sqrt{6}\cos\phi; \qquad \phi = \tfrac{1}{3}\arccos\left(\sqrt{6W}\right); \qquad W = \frac{S_{ij}S_{jk}S_{kj}}{\left(S_{ij}S_{ij}\right)};$$

$U = \sqrt{S_{ij}S_{ij} + \tilde{\Omega}_{ij}\tilde{\Omega}_{ij}}$; $\tilde{\Omega}_{ij} = \Omega_{ij} - 2\varepsilon\omega_k$; $\Omega_{ij} = \bar{\Omega}_{ij} - \varepsilon\omega_k$; ω_k is angular velocity; $\bar{\Omega}_{ij}$ is time average rotation rate tensor observed in angular velocity reference frame; S_{ij}, S_{jk} and S_{kj} are time average strain rate respectively; u_i is variable of U; x_i is independent variable of control equation of turbulent flow energy dissipation rate; η, c_1 and c_2 are coefficients, and the calculation formula is: $\eta = \dfrac{Sk}{\varepsilon}$, $c_1 = \max\left\{0.43, \dfrac{\eta}{5+\eta}\right\}$, c_2 = 5.0, σ_k = 1.2; ∂_ε = 1.0; S = $(2S_{ij}S_{ij})^{1/2}$; ν is turbulent velocity. In the realisable k–ε model, the governing equation of C_μ parameter and turbulent energy dissipation rate is as follows:

$$\begin{cases} C_\mu = \dfrac{1}{A_0 + A_s U\dfrac{k}{\varepsilon}} \\ \dfrac{\partial(\rho u_i \varepsilon)}{\partial x_i} = \dfrac{\partial}{\partial x_i}\left[\left(\eta + \dfrac{\eta_i}{\sigma_k}\right)\dfrac{\partial_\varepsilon}{\partial x_i}\right] + c_1\rho S\varepsilon - c_2\rho\dfrac{\varepsilon^2}{k+\sqrt{v\varepsilon}} \end{cases} \tag{1}$$

2.4 Turbulence model selection

In this study, the wind flow is set as high Reynolds number flow, so the wall function method is used to deal with the turbulent state of building surface. The generation and dissipation of turbulent kinetic energy in the near wall control unit are the same when the equilibrium assumption is added to the standard wall function. In practice, due to the influence of many factors, the specific turbulence state deviates from the above hypothesis. Therefore, the non-equilibrium wall function method is used in this study (Yisong et al., 2018). The non-equilibrium wall function method takes the pressure gradient and deviation into account, which makes the calculation more accurate for complex flows such as impact, encirclement and separation.

In the non-equilibrium wall function method, it is assumed that $\tilde{U} = U - \dfrac{1}{2}\dfrac{dp}{dx}\left[\dfrac{y_v}{\rho\kappa\sqrt{k}}\ln\left(\dfrac{y}{y_v}\right) + \dfrac{y-y_v}{\rho\kappa\sqrt{k}} + \dfrac{y_v^2}{\mu}\right]$;

$y_v \equiv \dfrac{\mu y_v^*}{\rho C_\mu^{1/4} k_p^{1/2}}$; $y_v^* = 11.225$; μ is the dynamic viscosity. The exponential rate of average velocity distribution is expressed as follows:

$$\frac{\tilde{U}C_\mu^{1/4}k^{1/2}}{\tau_w/\rho} = \frac{1}{\kappa}\ln\left(E\frac{\rho C_\mu^{1/4}k^{1/2}}{\mu}\right) \tag{2}$$

This method is quite different from the standard wall function method. It needs to solve the turbulent kinetic energy in the near wall element and considers it to be in accordance with two-layer distribution, i.e., complete turbulent layer and viscous bottom layer (Pan et al., 2020).

The distribution of turbulence correlation is as follows.

$$\tau_t = \begin{cases} 0 & y < y_v \\ \tau_w & y > y_v \end{cases} k = \begin{cases} \left(\dfrac{y}{y_v}\right)^2 k_p & y < y_v \\ k_p & y > y_v \end{cases} \varepsilon = \begin{cases} \left(\dfrac{2\nu k}{y^2}\right)^2 k_p & y < y_v \\ \dfrac{k^{3/2}}{C_l y} & y > y_v \end{cases} \tag{3}$$

where, $C_l = \kappa C_\mu^{-3/4}$, according to the above distribution assumption, the average generation terms k, $\bar{G}_k$ and dissipation rate $\bar{\varepsilon}$ in the near wall element are calculated. The expression is

$$\overline{G}_k \equiv \frac{1}{y_n}\int_0^{y_n} \tau_t \frac{\partial U}{\partial y} dy = \frac{1}{\kappa y_n} \frac{\tau_w^2}{\rho C_\mu^{1/4} k_P^{1/2}} \ln\left(\frac{y_n}{y_v}\right) \tag{4}$$

In equation (4), y_n is the height of the unit body, $y_n = 2y_p$.

$$\overline{\varepsilon} \equiv \frac{1}{y_n}\int_0^{y_n} \varepsilon dy = \frac{1}{y_n}\left[\frac{2v}{y_v} + \frac{k_p^{1/2}}{C_l} \ln\left(\frac{y_n}{y_v}\right)\right] k_P \tag{5}$$

It can be seen from equation (4) and equation (5) that the turbulent kinetic energy of near wall unit and the ratio of complete turbulent layer to viscous bottom layer are closely related, while the ratio of complete turbulent layer to viscous bottom layer is not fixed in unbalanced turbulence, and the variation range is relatively wide and dry. Therefore, the non-equilibrium wall function method can solve the influence of non-equilibrium effect on turbulent kinetic energy.

2.5 Grid generation

The calculation area refers to the selected area, including high-rise buildings, atmospheric boundary layer, etc. The size of the calculation area directly affects the length of numerical simulation calculation time and the accuracy of the calculation results (Duran et al., 2018). In addition, the location of high-rise buildings in the calculation area will also affect the results of numerical simulation (Li et al., 2018b). Therefore, the determination process of calculation area is introduced in detail.

In the process of numerical simulation of wind load on the surface of high-rise buildings along the street, the blocking ratio is used to measure the size of the calculation area, δ is the blocking rate, in the reduced high-rise building model, its value should be less than 3%; A_b is the windward area of the high-rise building along the street; A_d is the cross-sectional area of the calculation area. The blocking rate is defined as:

$$\delta = \frac{A_b}{A_d} \times 100\% \tag{6}$$

In order to facilitate the numerical simulation, it is necessary to set several walls at a distance from the high-rise building to ensure the closure of the solution domain. According to the above rules, the length, width and height of the calculation area are 2,800 m, 1,200 m and 1,200 m respectively. The high-rise building is located at the front 1/3 of the calculation area, and its windward, leeward, side and top surface meet the requirements.

The grid division in the calculation area also greatly affects the accuracy of numerical simulation results. In the high-rise building structure, the flow parameters along the normal direction of the wall surface change violently, so the grid needs to be densified. Based on this, the pressure in the inner boundary layer can be solved accurately (Yan et al., 2018).

In general, there are two kinds of grid forms: structured grid and unstructured grid. Among them, in the structured grid form, the nodes are arranged orderly, the relationship between adjacent nodes is clear, and the grid shape can not be determined, so the high-rise building can not be encrypted; in the unstructured grid form, the grid structure and topological connection are irregular, which has good adaptability and flexibility. Compared with the structured grid, the dense grid is more simple and more effective in complex boundary flow field problems in the region with large variation range (Xiong et al., 2018).

Figure 2 Diagram of grid division (see online version for colours)

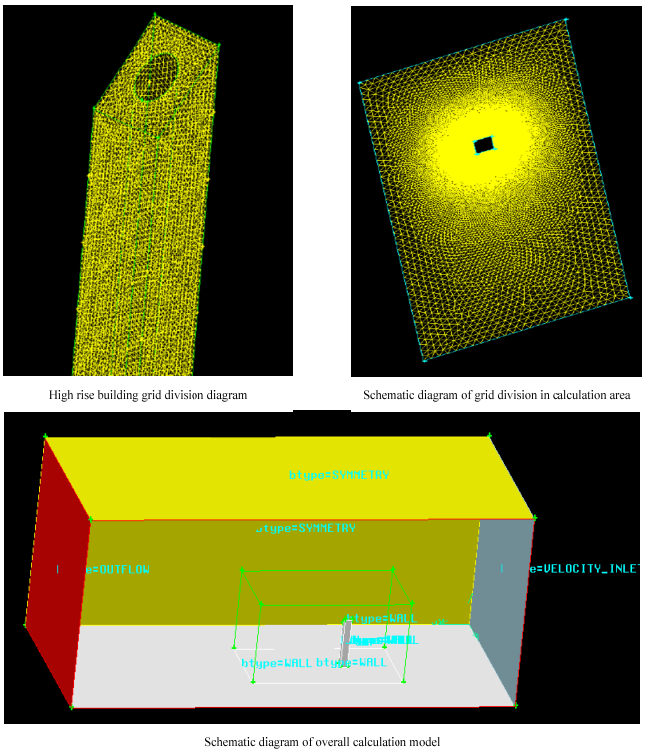

Schematic diagram of overall calculation model

In this paper, the research object belongs to a large and complex structure. Therefore, unstructured grid generation is used to grid the surrounding fluid, and a rectangular sub domain is set up around the high-rise building. In this region, the local grid encryption method is used to divide it into dense grids. Outside the region, the sparsity of the grid from the building surface to the boundary of the computational domain gradually increases (Cheng and Li, 2018). The grid division diagram is shown in Figure 2.

The above process completes the determination of the calculation area, and carries on the grid division to prepare for the calculation and solution of the final turbulence model.

The surrounding fluid is meshed, and the local grid densification method is adopted, that is, a 950 m × 500 m × 500 m rectangular subdomain is set up around the building. A denser grid is used in this subdomain, and a sparser grid is used outside the subdomain. The grid gradually increases from the building surface to the boundary of the computing domain. After the grid is divided, a total of nearly 2.1 million tetrahedral grids are generated.

2.6 Numerical simulation of wind load

The correct setting of boundary conditions is the most critical step in the process of model calculation and solution. According to the requirements of numerical simulation of wind load on the surface of high-rise buildings along the street, the boundary conditions are set as follows:

1 the velocity inlet is used to set the inlet boundary conditions

Let $V(z)$ be the wind speed profile of atmospheric boundary layer, V_{10} be the reference wind speed under the standard landform, H_0 be the gradient wind height under the standard landform, Z be the arbitrary height under the D landform, H_α be the gradient wind height under the D landform, and α be the ground roughness coefficient of the D landform. The calculation formula of wind speed profile in atmospheric boundary layer is as follows:

$$V(z) = V_{10}\left(\frac{H_0}{10}\right)^{0.16}\left(\frac{Z}{H_\alpha}\right)^{0.30} \tag{7}$$

The calculation formula of turbulence intensity is as follows:

$$I_z = 0.15\left(\frac{Z}{H_\alpha}\right)^{-0.05-\alpha} \tag{8}$$

The calculation formula of turbulent kinetic energy is as follows

$$k = \frac{3}{2}(uI_z)^2 \tag{9}$$

The calculation formula of dissipation rate is

$$\varepsilon = C_\mu^{3/4}\frac{k^{3/2}}{l} \tag{10}$$

2 the pressure outlet is used to set the boundary conditions of the outflow surface

3 symmetrical boundary conditions are used to set the parameters of the top and both sides of the basin

4 the surface parameters of high-rise buildings are set by the condition of no sliding wall.

According to the above selected turbulence model and the set boundary conditions, the turbulence model is calculated and solved by the separate solver. The specific process is as follows.

The flow field around a high-rise building is determined by encirclement, impact, separation and vortex. For complex flow, such as high flow imbalance and large pressure gradient, the non-equilibrium wall function can be used to obtain better results. Due to the existence of the wall will affect the flow field, leading to the complex phenomenon of backflow, reverse pressure gradient and so on, the above phenomenon is corrected by non-equilibrium wall function, based on which, the flow phenomenon of airflow and load around high-rise building is simulated (Xiao et al., 2018).

The speed and accuracy of the numerical simulation results depend on the discrete scheme of the computational region. Through comparative study, it is found that the first-order accuracy discrete scheme is easy to converge, but this discrete scheme contains more numerical dissipation. In the process of quantitative analysis, the application of this discrete scheme should be reduced as much as possible. The accuracy of the second-order upwind scheme is high, which can be obtained in the numerical discretisation process of turbulent kinetic energy and dissipation rate. However, this kind of discrete scheme is easy to lead to the divergence of numerical calculation, resulting in the instability of the calculation process, thus affecting the accuracy of the calculation results. Therefore, it is necessary to select a smaller relaxation coefficient in the application process of this discrete scheme (Jo et al., 2018).

According to the above analysis process, in order to quantitatively analyse the effect of wind load on the surface of high-rise buildings along the street, the second-order upwind scheme with small relaxation coefficient is adopted to greatly accelerate the convergence speed (Shi, 2019). In addition, after many times of trial calculation, the value of under relaxation coefficient of pressure is 0.2, the value of other items is 0.5, and the standard value of residual convergence is 0.0001.

In this study, the flow around the bluff body is incompressible at low speed. Therefore, a separate solver is used, and the scheme is implicit and steady. The air density is constant, the value is 1,225 kg/m^3, and the dynamic viscosity μ is 1.7894 10^{-5}N•s/m^2.

In this process, BIM model is used to simulate the wind load on the surface of high-rise buildings along the street, which provides a new means to support the research on the influence of wind load on high-rise buildings (Sun et al., 2019).

3 Numerical simulation experiment of wind load on high-rise buildings along the street

3.1 Selection of experimental objects

In order to verify the effectiveness of the numerical simulation method of wind load on the surface of high-rise buildings along the street, MATLAB software is used to design the simulation experiment. The specific experimental process is shown as follows.

A high-rise building along the street in a city is selected as the experimental object. The building number is building 11. The east side of the high-rise building is the street, without any obstruction. There are few high-rise buildings nearby and the vision is very wide. The experimental object is a high-rise building with 37 floors and a height of 146 m.

In order to obtain the distribution law and characteristics of wind pressure on the surface of high-rise buildings along the street, 20 wind pressure test points are arranged around the 33rd floor of the experimental object. In the

experimental test stage, due to the strong wind force, the sensors at No. 2, 17, 19 and 20 are leaked out, and the sensors at 12, 13, 15 and 18 are faulty, and the remaining 12 effective sensors are finally detected.

The experimental object, wind pressure sensor and the arrangement of measuring points are shown in Figure 3.

Figure 3 Experimental object, wind pressure sensor and layout of measuring points (see online version for colours)

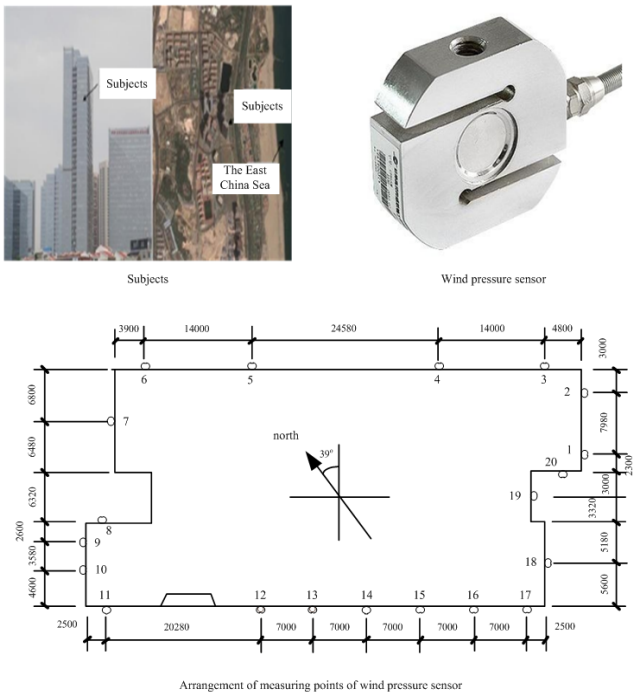

The above process completes the selection of experimental objects, and selects the appropriate wind pressure sensor and its measuring points, which laid a solid foundation for the simulation experiment.

3.2 Experimental parameter setting

In order to ensure the smooth progress of the simulation experiment, the simulation experiment parameters are set, mainly including the calculation area size, griding parameters and boundary conditions, etc. The specific parameter setting process of simulation experiment is as follows.

The geometric model of the experimental high-rise buildings along the street is constructed with a scale of 1: 300. According to the above scale ratio, the relevant physical quantities are obtained as shown in Table 2.

In the experiment, ICEM is used to grid the high-rise buildings along the street. In order to facilitate the construction of geometric model, the full size of the experimental object is input into ICEM, and the scale operation is performed at the same time of griding calculation.

Table 2 Physical quantities related to geometric model of high-rise buildings along the street

Physical quantity	*Scale ratio*	*Physical quantity*	*Scale ratio*
Length	1:300	Acceleration	300:1
Density	1:1	Power	1:3002
Time	1:300	Pressure (force/area)	1:1
Speed	1:1		

The size of the calculation area directly affects the accuracy of the numerical simulation results. If the size of the calculation area is too large, the number of grids will increase and the calculation time will be prolonged; if the size of the calculation area is too small, the number of grids will be reduced and the calculation granularity will be insufficient.

Therefore, according to the existing literature research results, the calculation area size is set. The calculation area size is shown in Table 3.

Table 3 Calculation area size table

Calculation area	*Original size (m)*	*Scale size (m)*
Calculate area entrance to building	800	2.667
Building to calculation area exit	2,100	7.000
Building to both sides of calculation area	600	2.000
Building to top of calculation area	350	1.167

Figure 4 Grid division of high-rise buildings along the street

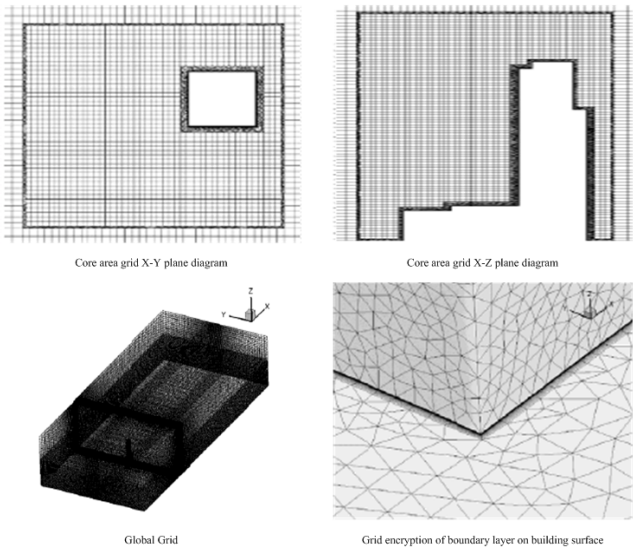

According to the data in Table 3, the model of high-rise buildings along the street is grided. The grid division diagram is shown in Figure 4.

The setting of calculation area boundary conditions is also a key factor affecting the accuracy of numerical

simulation results. Therefore, the calculation area boundary conditions are set according to the actual situation, as shown in Table 4.

Table 4 Setting table of boundary conditions of calculation area

Calculate area boundary	*Boundary conditions*	*Boundary conditions (Chinese)*
Calculation area entrance	Velocity-inlet	Speed inlet
Calculate regional exports	Pressure-outlet	Pressure outlet
Calculation area side	Symmetry	Symmetric boundary
Top surface of calculation area	Symmetry	Symmetric boundary
Calculation area surface	No-slip wall	Slip free wall

The above process completes the setting of experimental parameters and provides data support for the experiment.

With the support of the above experimental parameters and experimental conditions, the overall experimental scheme is set as follows: Taking the wind pressure coefficient error, simulation efficiency and simulation accuracy as the experimental comparison indexes, the proposed method is compared and verified with the methods of Lv and Liu (2019), Chen et al. (2019) and Zheng et al. (2018).

1 Wind pressure coefficient error: the lower the error of the simulated wind pressure coefficient is, the higher the accuracy of the simulation results is, and the simulation method is more effective.

   In order to facilitate the comparison and analysis of the experimental results, the numerical simulation results are converted into wind pressure coefficient.

$$C_{pi} = \frac{P_i - P_\infty}{0.5\rho V_\infty^2} \tag{11}$$

   In equation (11), C_{pi} is the wind pressure coefficient of a measuring point i on the surface of high-rise buildings along the street; P_i is the wind pressure value of measuring point i; P_∞ is the static pressure value of reference point; V_∞ is the wind speed of reference point, which is set as 33.3 m/s in this experiment.

2 Simulation efficiency: simulation efficiency refers to the ratio of simulation workload and simulation time of different methods for the same experimental conditions. Therefore, the higher the simulation efficiency, the better the performance of the simulation method.

3 Simulation accuracy: simulation accuracy refers to the ratio of wind load simulation results of different methods to actual wind load results. Therefore, the higher the simulation accuracy, the better the performance of the simulation method.

3.3 Error results of wind pressure coefficient

The performance of numerical simulation method is mainly reflected by the error of wind pressure coefficient. The smaller the error of wind pressure coefficient is, the better the performance of numerical simulation method is. In order to show the error of wind pressure coefficient more intuitively, the surface of high-rise buildings along the street is divided into 13 equal blocks. The error data of wind pressure coefficient obtained by simulation experiment are shown in Table 5.

Under normal conditions, the error of wind pressure coefficient calculated by numerical simulation is less than 10%, which indicates that the accuracy of numerical simulation is high. As shown in Table 5, the block wind pressure coefficients obtained by different wind directions are very close to the actual measured values, and the average error is less than 10%. Among them, the data with large error of wind pressure coefficient is generally the block with the largest positive wind pressure on the windward side, and the bias value is about 25%.

The experimental results show that the average error of wind pressure coefficient of the proposed numerical simulation method is less than 10%, which fully shows that the proposed numerical simulation method has good performance.

3.4 Simulation efficiency comparison results

The simulation efficiency comparison results of the four methods are shown in Figure 5.

Figure 5 Simulation efficiency comparison results

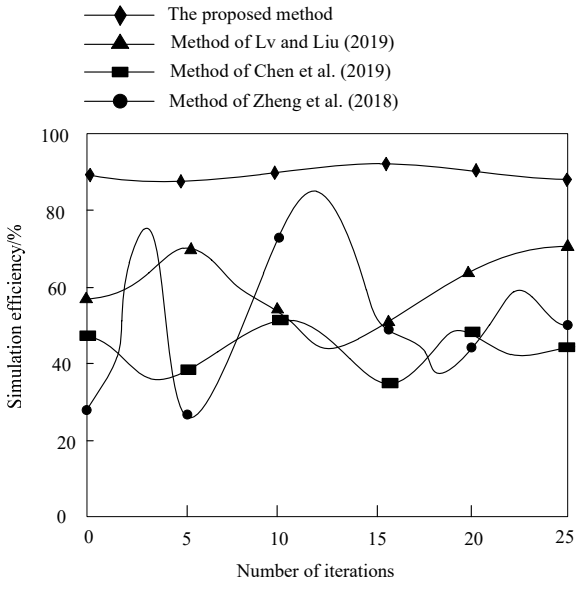

As can be seen from Figure 5, with the increasing number of iterations, the simulation efficiency of the proposed method always maintains a high level, while the simulation efficiency of the three literature comparison methods fluctuates obviously and the simulation efficiency is low. The simulation efficiency will not be affected by the relevant configuration. The computer conditions in different

experimental environments are the same as the algorithm conditions. Since the calculation formula of efficiency is the ratio of workload to working time, the relevant configuration will not affect the simulation efficiency.

3.5 Simulation accuracy

Simulation accuracy is the most critical performance of simulation methods. Therefore, taking simulation accuracy as the experimental comparison index, this method is compared with three traditional methods. The simulation accuracy comparison results of this method with Lv and Liu (2019), Chen et al. (2019) and Zheng et al. (2018) are shown in Figure 6.

From the simulation accuracy comparison results in Figure 6, it can be seen that the simulation accuracy of the method in this paper has always maintained a high level, and the highest simulation accuracy of the method in this paper has reached 96%. The simulation accuracy of the three literature comparison methods fluctuates greatly, showing a trend of increasing first and then decreasing. Although the simulation accuracy of the three traditional literature comparison methods has increased, the highest simulation accuracy of the three methods reaches 90%, and the lowest value is even less than 50%. Therefore, this method has high simulation accuracy.

Figure 6 Comparison results of simulation accuracy

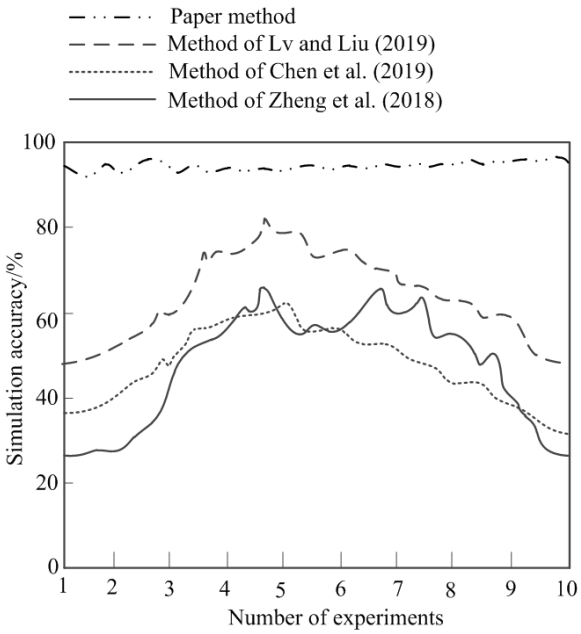

Table 5 Error data table of wind pressure coefficient

No.	*Wind angle 0°*			*Wind angle 45°*		
	Simulation value	*Actual measured value*	*Error*	*Simulation value*	*Actual measured value*	*Error*
1	–0.46	–0.50	0.08	–0.41	–0.46	0.11
2	–0.40	–0.45	0.08	–0.42	–0.39	0.77
3	–0.50	–0.55	0.09	–0.33	–0.35	0.06
4	–0.49	–0.63	0.22	–0.19	–0.20	0.05
5	–0.57	–0.61	0.06	–0.29	–0.35	0.17
6	–0.56	–0.60	0.67	–0.15	–0.15	0.00
7	–0.70	–0.69	0.01	–0.25	–0.30	0.17
8	–0.56	–0.56	0.00	–0.16	–0.15	0.07
9	–0.71	–0.72	0.01	–0.21	–0.21	0.00
10	–0.78	-0.85	0.08	–0.10	–0.10	0.00
11	0.25	0.25	0.00	0.25	0.20	0.25
12	0.23	0.25	0.08	0.15	0.25	0.4
13	0.24	0.24	0.0	0.12	0.12	0.00
No.	*Wind angle 90°*			*Wind angle 135°*		
	Simulation value	*Actual measured value*	*Error*	*Simulation value*	*Actual measured value*	*Error*
1	–0.53	–0.46	0.15	–0.41	–0.43	0.05
2	–0.38	–0.34	0.11	–0.26	–0.31	0.16
3	–0.52	–0.42	0.14	–0.42	–0.43	0.02
4	–0.43	–0.39	0.10	–0.43	–0.33	0.30
5	–0.48	–0.41	0.17	–0.36	–0.41	0.12
6	–0.41	–0.39	0.05	–0.36	–0.48	0.25
7	–0.38	–0.36	0.56	–0.30	–0.42	0.19
8	–0.37	–0.35	0.57	–0.21	–0.32	0.34

Table 5 Error data table of wind pressure coefficient (continued)

No.	*Wind angle 0°*			*Wind angle 45°*		
	Simulation value	*Actual measured value*	*Error*	*Simulation value*	*Actual measured value*	*Error*
9	–0.33	–0.34	0.29	–0.24	–0.32	0.25
10	–0.30	–0.36	0.17	–0.21	–0.30	0.30
11	–0.08	–0.10	0.2	–0.38	–0.33	0.15
12	–0.15	–0.18	0.17	–0.32	–0.32	0.00
13	–0.15	–0.20	0.25	–0.29	–0.32	0.09

4 Conclusions

In order to improve the accuracy of wind load simulation of high-rise buildings along the street and improve the safety of buildings, a research method for numerical simulation of wind load on the surface of high-rise buildings along the street based on BIM model is proposed. The following conclusions are proved from both theoretical and experimental aspects. This method has lower simulation accuracy and higher simulation efficiency in the numerical simulation of wind load on high-rise buildings along the street. Specifically, the maximum simulation error of the proposed method is 0.4 under the four wind directions; compared with the finite element analysis method based on ANSYS, the simulation efficiency is significantly improved, and the maximum simulation efficiency can reach 92%. Therefore, it fully shows that the simulation method based on BIM model can better meet the requirements of numerical simulation of wind load on the surface of high-rise buildings along the street.

References

Caroline, J. and Muller, D.M. (2018) 'Romps. acceleration of tropical cyclogenesis by self-aggregation feedbacks', *Proc. Natl. Acad.*, USA, Vol. 115, No. 12, pp.2930–2935.

Chen, Y.Y., Liu, W.B., Yuan, Y., Kong, G. and Gao, J.W. (2019) 'Research on three-dimensional deformation measurement for glass curtain wall under wind load by the technique of DPDM', *China Measurement and Testing Technology*, Vol. 45, No. 6, pp.29–34.

Cheng, J. and Li, L. (2018) 'Simulation research on heat preservation and energy saving control of residential building wall', *Computer Simulation*, Vol. 35, No. 6, pp.250–253.

Duran, R., Beron-Vera, F.J. and Olascoaga, M.J. (2018) 'Extracting quasi-steady Lagrangian transport patterns from the ocean circulation: an application to the Gulf of Mexico', *Rep,* Vol. 8, No. 1, pp.5218–5218.

Jo, J.H., Choi, J.U., Konarov, A. and Yashiro, H. (2018) 'Sodium-lon batteries: building effective layered cathode materials with long-term cycling by modifying the surface via sodium phosphate', *Advanced Functional Materials*, Vol. 28, No. 14, pp.1–11.

Li, M., Qi, T., Bernabé, Y., Zhao, J.Z., Wang, Wang, D. and Wang, Z.M. (2018a) 'Simulation of solute transport through heterogeneous networks: analysis using the method of moments and the statistics of local transport characteristics', *Rep*, Vol. 8, No. 1, pp.3780–3780.

Li, X., Chang, S. and Leng, M. (2018b) 'Numerical simulation of water droplet parameters variation along the icing wind tunnel', *Computer Simulation*, Vol. 35, No. 10, pp.66–71.

Lv, C.L. and Liu, Y.J. (2019) 'Research on the wind load for the detached eddy simulation of super high-rise buildings', *Building Science*, Vol. 35, No. 7, pp.90–96.

Mansur, A., Hird, M.A., Desimone, A., Pshonyak, S., Tom, A. and Das, U. (2018) 'Driving habits and behaviors of patients with brain tumors: a self-report, cognitive and driving simulation study', *Rep*, Vol. 8. No. 1, pp.4635–4635.

Mohammadi-Aragh, M., Goessling, H.F., Losch, M. and Hutter, N. (2018) 'Predictability of Arctic sea ice on weather time scales', *Scientific Reports*, Vol. 8, No. 1, pp.2045–2322.

Pan, L., Zhang, H., Lu, S. and Chen, Y.H. (2020) 'Effect of pressure on boundary slip of thin film lubrication using atomistic simulation', *Journal of Wuhan University of Technology-Mater Sci. Ed*., Vol. 35, No. 1, pp.47–52.

Shi, H. (2019) 'Simulation study on vulnerability of tunnel structure under insufficient lining thickness', *Computer Simulation*, Vol. 36, No. 7, pp.230–233+375.

Shu, Y., Qi, L., Song, Q. and Wang, C. (2019) 'Simulation of tensile behaviors of bamboo-like carbon nanotubes based on molecular structural mechanics approach combining with finite element analysis', *Journal of Wuhan University of Technology Mater. Sci. Ed.,* Vol. 34, No. 1, pp.11–16.

Sun, X., Jovanovic, J., Zhang, Y., Chu, Y.H., Mo, Y.J. and Liao, S.G. (2019) 'Use of encapsulated phase change materials in lightweight building walls for annual thermal regulation', *Energy*, Vol. 180, No. 1, pp.858–872.

Wang, C., Liu, P., Wang, Y., Yuan, Z. and Xu, Z.H. (2018) 'Experimental study of key effect factors and simulation on oil displacement efficiency for a novel modified polymer BD-HMHEC', *Rep*, Vol. 8, No. 1, pp.3860–3860.

Xiao, Y., Taguchi, Y. and Kamat, V.R. (2018) 'Coupling point cloud completion and surface connectivity relation inference for 3D modeling of indoor building environments', *Journal of Computing in Civil Engineering*, Vol. 32, No. 5, pp.1–12.

Xiong, Y., He, A. and Quan, C. (2018) 'Security analysis of a double-image encryption technique based on an asymmetric algorithm', *J. Opt. Soc. Am. A. Opt. Image Vis*., Vol. 35, No. 2, pp.320–326.

Yan, X., Li, B. and He, Y. (2018) 'Research on the anti-galloping of transmission lines based on the influence of impact load', *Computer Simulation,* Vol. 35, No. 12, pp.77–80, 301.

Yisong, X., Zhengqiang, L., Li, L., Richard, W., Ihab, A., Kaitao, L., Donghui, L., Ying, Z., Xingfeng, C. and Hua, X. (2018) 'Aerosol optical, microphysical, chemical and radiative properties of high aerosol load cases over the Arctic based on AERONET measurements', *Rep*, Vol. 8, No. 1, pp.9376–9376.

Zheng, X.L., Xiong, J.M., Zhou, J.Z. and Shu, Z. (2018) 'Parametrization study of ring expanded symmetrical cable net structure based on ANSYS finite element method', *Science Technology and Engineering*, Vol. 18, No. 11, pp.281–286.